Available online at www.sciencedirect.com
ScienceDirect
Ceramics International 35 (2009) 803–811
CERAMICS INTERNATIONAL
www.elsevier.com/locate/ceramint

Screen printing of sol–gel-derived electrolytes for solid oxide fuel cell (SOFC) application

Ralf Hansch [1], Mohammad Rahul Reza Chowdhury, Norbert H. Menzler *

Forschungszentrum Jülich GmbH, Institute of Energy Research IEF, IEF-1: Materials Synthesis and Processing, 52425 Jülich, Germany

Received 22 December 2007; accepted 22 February 2008
Available online 4 July 2008

Abstract

The idea of using the sol–gel technique for producing low-cost components for solid oxide fuel cell (SOFC) application has attracted great interest. Besides its economic advantages, the sol–gel technique additionally offers the chance to reduce either the thickness of the electrolyte and therefore to reduce ohmic resistances or to lower the sintering temperature of single components like the electrolyte layer, due to the clearly reduced particle sizes of colloidal distributed particles in the sol.

The work presented here deals with the development of sols and their application in combination with yttria fully stabilized zirconia mixed-oxide powders for the preparation of screen-printing pastes. Besides physical, chemical and thermal characterization of the sols, variations of the composition of the sol as well as of the pastes composed of sol and mixed-oxide powder were evaluated for preparing dense, gas-tight layers sintered at various temperatures, resulting in sufficient gas-tightness to ensure high power density SOFCs. Additionally, technological screen-printing parameters were studied.

Single cell tests (50 mm × 50 mm) revealed current densities of approx. 1 A/cm^2. These values are comparable to current densities obtained by cells based on normal electrolyte layers, which were prepared in parallel.

Keywords: Sol-gel processes; Fuel cells; Electrolyte; Screen printing

1. Introduction

Currently, the most advanced methods for the preparation of the electrolyte layer in the planar solid oxide fuel cell (SOFC) system are wet chemical coating technologies like vacuum slip casting (VSC) or screen printing using mixed oxide based slurries [1–6]. However, thermal coating techniques like atmospheric or vacuum plasma spraying are already under development [7,8]. A common problem of the mixed oxide based wet chemical coated electrolyte layers is the relatively high sintering temperature of about 1400 °C to ensure gas-tightness. Based on the low processing temperatures, sol–gel materials offer a new way to reduce sintering temperatures. Unfortunately, due to the high amount of organic components as well as the high sintering activity of the nanosized particles in the sol only layers with a thickness in the range of a few hundred nanometers could be produced without the formation of cracks or delamination. If sols were used to prepare electrolyte layers on typical anodes of anode-supported SOFCs, no complete layers could normally be obtained due to the mismatch between surface roughness of the anode (∼0.5–2 μm; representing the particle and pore size of the anode) and the thickness to be reached by a sol layer or layers with nanocrystallized starting materials (≪0.5 μm) [9,10]. Typically either after drying or after sintering, those layers cracked or delaminated. To overcome those problems a new approach is taken in this work by preparing a screen-printing paste from a mixture of a sol–gel precursor and a mixed-oxide powder. This method offers the opportunity to combine the high sintering activity of the sol–gel material with the ability of mixed-oxide slurries to produce crack-free layers with a thickness in the range of a few micrometers. In the following, the characterization of the starting materials, the optimization of the screen-printing slurries and printing techniques will be presented as well as the results of the sintering experiments for the electrolyte layers.

* Corresponding author at: Forschungszentrum Jülich, IWV-1, 52425 Jülich, Germany. Tel.: +49 2461 61 3059; fax: +49 2461 61 2455.
E-mail address: n.h.menzler@fz-juelich.de (N.H. Menzler).
[1] Present address: North Rhine-Westphalia Office of Criminal Investigation (Landeskriminalamt NRW), SG51.1, 40221 Düsseldorf, Germany.

0272-8842/$34.00
doi:10.1016/j.ceramint.2008.02.020

2. Experimental

2.1. Substrates

For the experiments planar anode substrates were prepared according to the Research Center Jülich's SOFC concept. The complete manufacturing steps are presented elsewhere [11], and only a short description is given here. An anode cermet composed of 57 wt.% nickel oxide and 43 wt.% 8YSZ (with 8 mol% yttria stabilized zirconia; cubic crystallography) is used as the substrate material. The raw materials modified by the Coat-Mix® [12] process were warm-pressed and subsequently debindered and sintered at 1230 °C for 3 h. After this step the substrate (340 mm × 340 mm) was cut into pieces of 50 mm × 50 mm by diamond blade sawing. After cutting, a thin anode (5–7 μm), composed of the same materials as the substrate itself, but with a finer particle size was added via the vacuum slip casting process (VSC). After a second sintering step at 1000 °C for 1 h to ensure adherence, these samples were used for all subsequent coating experiments.

2.2. Preparation of the raw materials

The basic material for all pastes consisted of 8YSZ powder (TZ-8Y) from Tosoh, Japan, which was pre-calcined in a first step at 1240 °C for 3 h. After cooling down to 200 °C, the material was stored in a desiccator with P_2O_5 as the drying agent. In a second step the powder was milled with acetone in a ball mill for 120 h to achieve grain sizes between 0.5 and 1 μm. The grain size was checked by a laser particle size analyzer (Fritsch Analysette). Afterwards the material was dried in a vacuum desiccator at a pressure of less than 100 h Pa and temperatures between 20 and 100 °C to avoid the formation of hard agglomerates.

The preparation of the sol used in this study is based on a patent by Barrow et al. [13,14]. The raw materials are zirconium *n*-propoxide 70 wt.% in propanol, yttrium nitrate $Y(NO_3) \times 5H_2O$, pure carboxylic acid (acetic, propanoic, caproic or nonanoic acid), acetylacetone and distilled water. A solution of acetylacetone and the carboxylic acid was added to the zirconium *n*-propanol. Stoichiometric amounts of yttrium nitrate dissolved in distilled water were introduced dropwise at 0 °C to obtain pure cubic 8YSZ phase. To ensure that the hydrolysis–condensation reaction is complete, the amount of water added was four times greater than the stoichiometric amount in comparison to the alkoxide. The maximal 8YSZ wt.% content in each sol was limited by the fixed molar ratios of the acetylacetone/zirconium *n*-propoxide/carboxylic acid, and yielded maximum 8YSZ contents of 20 wt.% (acetic acid), 19 wt.% (propanoic acid), 18 wt.% (caproic acid) and 17 wt.% (nonanoic acid), respectively.

2.3. Paste preparation and screen printing

For the preparation of the screen-printing pastes without a binder, 8YSZ/sol ratios from 20/80 to 40/60 wt.% were premixed by hand. Further homogenization was conducted using a three-roll mill by scaling down the milling gap in several individual steps. In order to complete homogenization this step was repeated three times. A typical additive containing 94 wt.% terpineol and 6 wt.% ethylene cellulose was used for the preparation of pastes with a binder and also for a typical internal paste for comparison, which was prepared from the mixed-oxide powder only.

Three different types of meshes with mesh sizes of 34, 43 and 65 μm were evaluated for printing the electrolyte. Although the two meshes with a mesh size of 43 and 65 μm showed good results, all further experiments were conducted with the 43 μm mesh, due to the expected smaller thickness of the printed layer. Additionally, two different printing techniques were chosen, a uniaxial and a transposed technique where the substrate is rotated by 90° before the squeegee returns to the starting position. All samples have dimensions of 50 mm × 50 mm.

2.4. Sintering and testing

Sintering of all the printed electrolyte layers was conducted at temperatures of 1400 or 1350 °C and a dwelling time of 5 h. In all cases an ironing step was performed at a temperature 50 °C lower than the sintering temperature to minimize bending of the samples due to the different shrinking behavior of the electrolyte and the substrate. At the electrolyte densification temperature the substrate is still porous, therefore the material continues to shrink. As a result of this shrinking mismatch (or mismatch in sintering behavior) the samples bent convexly. The ironing step considerably reduces this mismatch bending. After cooling to room temperature, there is only some slight warpage due to differences in the coefficients of thermal expansion of the electrolyte material (approx. $10.5 \times 10^{-6}\,K^{-1}$) and the substrate material (approx. $12–12.5 \times 10^{-6}\,K^{-1}$).

The gas-tightness of the electrolytes was estimated by a helium leak test. The values presented were first measured at a pressure difference of approx. 1000 h Pa and then calculated by taking the area of the sample and a pressure difference of 100 h Pa (a typical pressure difference between air and fuel side within an SOFC stack) into account. An internal threshold value of 2.0×10^{-5} h Pa $dm^3/s\,cm^2$ was used as a quality attribute for the gas-tightness of the electrolyte. This value represents the amount of carrier gas (volume; here He) which could diffuse in a given time (s) per area to be measured (cm^2) at a given pressure difference on both sides (h Pa).

3. Results

3.1. Sol stability and characterization

In a first step, the stability of the sols prepared with different carboxylic acids and solid contents was investigated so that it was possible to produce sols with optimal conditions for the preparation of the pastes. A summary of the stabilities is given in Table 1.

It is clear that the higher the aliphatic chain of the carboxylic acid, the higher the sol stability. In fact, when nonanoic acid

Table 1
Summary of the screened synthesis compositions showing influence of solid content (wt.%) and type of carboxylic acid on the final sol stability

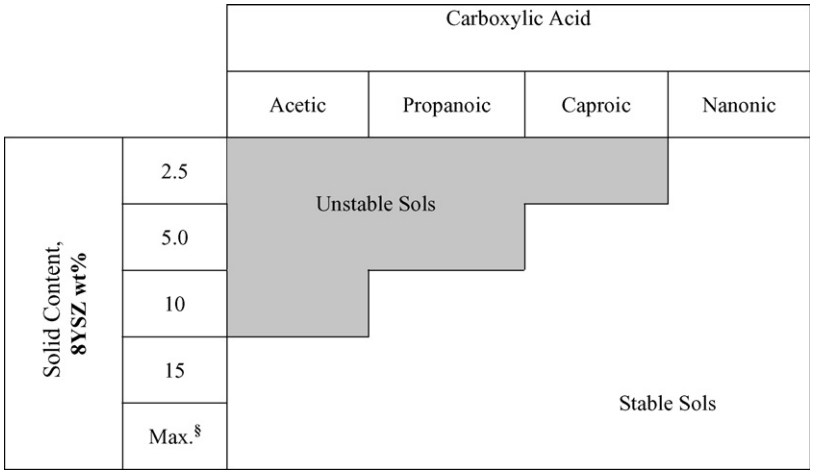

Shaded cells represent unstable sols while white ones represent stable clear sols (stable for several months).

was used, the sols were stable in the whole range of the chosen solid contents. Since the carboxylic acid acts as a hydrolysis/polymerization catalyst, this behavior can be explained considering that the lower acid strength of long-chain acid reduces the reaction (growth) rate, decreasing in turn the formation of bigger particles and agglomerates, which finally destabilize the sol. Moreover, another effect which must be taken into account is that when increasing the acid chain length, the YSZ nanoparticles are somehow better protected or capped [15], thus reducing the possibility of agglomeration. Stable sols showed a similar particle size distribution with an average particle diameter of 7 nm, measured with dynamic laser-scattering equipment.

Especially for screen-printing pastes, the rheology of the basic sol plays an important role in the paste quality. Therefore, the viscosity of the sols prepared with different carboxylic acids were measured by rotation viscosimeter and a double gap measuring body. As can be seen from the rheology curves in Fig. 1, the viscosity of all sols is in the range of 1–10 mPa s, showing a slight increase of the viscosity with increasing chain length of the carboxylic acid. Despite this, the viscosity of all sols is independent of the shear rate in the range of 10 and 1000 s^{-1}, which is typical of a Newtonian liquid. A small thixotropic effect was observed in a few measurements, which can be related to the start of gelation occurring in the sols.

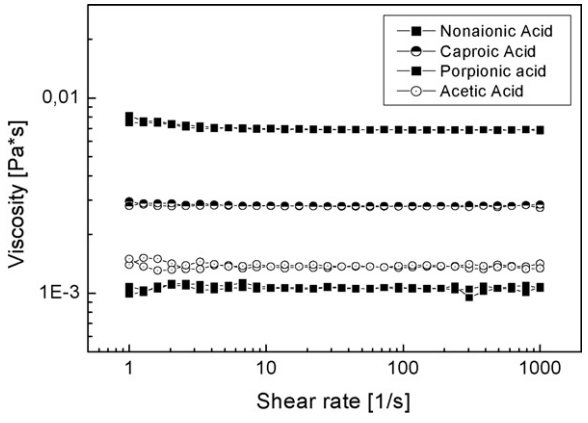

Fig. 1. Viscosity of the basic sols for the screen-printing pastes as a function of the aliphatic chain length of the carboxylic acid.

For the investigation of the thermal decomposition behavior of the sols, samples from every sol were dried at 50 °C for 24 h and analyzed in a coupled differential thermal analysis and thermogravimetric analysis (DTA/TGA) equipment. Fig. 2 shows a typical TGA/DTA analysis of a sol prepared using propanoic acid. The most important mass loss occurs between 200 and 260 °C. Especially at 255 °C a sharp mass loss (20 wt.%) and an intense exothermic peak can be seen, corresponding therefore to the burnout of most of the organics adsorbed or bound to YSZ particles. Other exothermic peaks can be observed at 350, 650 and 800 °C, combined with a progressive mass loss of 10 wt.% when the sols are heated from 300 to 900 °C. The latter peaks are associated with the progressive particle densification and sintering of the initial nanosized particles.

The chemical purity and the phase content of the starting materials are important to ensure good ionic conductivity. Control analysis by ICP–OES (inductively coupled plasma with optical emission spectroscopy) and X-ray analysis revealed that in all cases zirconia was fully stabilized with 8 mole% yttria (cubic structure). Small amounts of Al_2O_3 (0.2 wt.%), SiO_2 (0.01 wt.%) and TiO_2 (0.28 wt.%) could be related to impurities in the precursor Zr *n*-propoxide.

As can be seen from the XRD pattern (X-ray diffraction) in Fig. 3 as an example the sol is still amorphous after drying and heating to 300 °C. Crystallization starts at about 600–650 °C indicated by the occurrence of broad peaks in the pattern. At higher calcination temperatures, the diffraction peaks became sharper indicating crystallization and increasing crystallite growth. At 800 °C the material is mostly crystallized and of almost pure cubic phase, although the peaks are still broad, which can be attributed to the small crystallite size. Some diffuse peaks at low Bragg angles between 20 and 25° can be

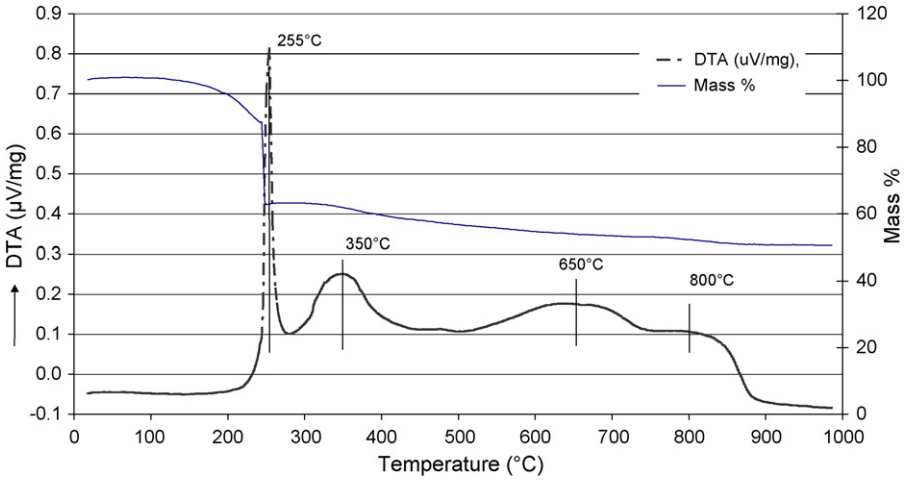

Fig. 2. TGA/DTA measurements of dried sols heated at a rate of 5 K/min in an air flow (50 ml/min). Prior to analysis the sol was dried at 50 °C for 24 h.

interpreted as residuals of the amorphous phase. The crystallite size calculated by the Debye–Scherrer formula from XRD patterns of powders calcined at 800 °C is 14 nm.

3.2. Paste formulation and characterization

As already described, screen-printing pastes of sol–gel and mixed-oxide powder with ratios between 20/80 and 40/60—gradually varied by 5 wt.% steps were prepared without an incorporated binder. Due to the criteria of homogeneity, only 5 different screen-printing pastes, listed in Table 2, were used for further printing experiments. Pastes with other ratios and sols were prepared, but eliminated because of their inhomogeneity (Fig. 4).

In order to investigate the behavior of the pastes during the screen-printing process, first printing experiments were performed on stainless steel substrates, using a mesh with a network mask. No visible differences could be observed when the sol to mixed-oxide powder ratio was changed. In contrast, pastes with identical ratio but different carboxylic acids incorporated in the basic sols exhibited different behavior. While pastes containing caproic acid show a sharply formed rim of the hexagonal mesh structure, pastes with nonanoic acid exhibit a frayed-out rim, due to their reduced flowability and the stronger adhesion to the steel substrate. However, for both pastes a very fast and uncontrolled drying behavior was recognized, which caused strongly structured morphologies in the printed areas.

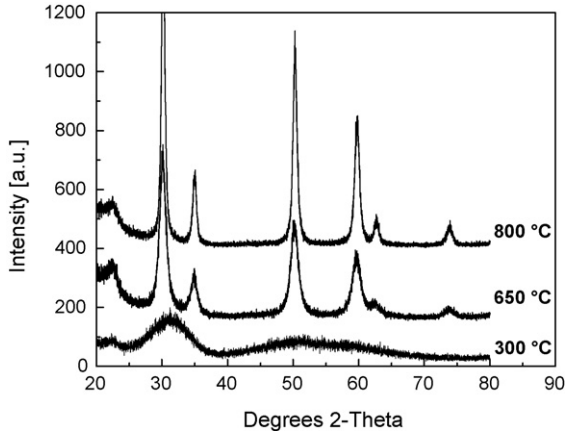

Fig. 3. Typical XRD diffractogram of a fully yttria stabilized sol, dried and calcined at different temperatures.

To minimize this uncontrolled drying, in the next series of pastes, ethyl cellulose and terpineol were introduced as the binder system. Additionally, a binder containing a ‘‘standard’’ paste without a sol was prepared from 100 wt.% mixed-oxide powder for comparison. In analogy to the investigations of the homogeneity of the pastes without a binder, a first evaluation of the homogeneity for these pastes with a binder system was made in order to prevent unnecessary experiments being performed. The composition of pastes with good homogeneity used for further experiments are shown in Table 3.

Due to the high influence of the viscosity, rheology measurements of the sol-based pastes were conducted in comparison to the ‘‘standard’’ paste. Starting at a shear rate of 1 s^{-1} the ‘‘standard’’ paste showed a higher viscosity at 200 Pa s than the sol-based pastes with approximately 40 Pa s. However, due to the high viscosity the curve of the ‘‘standard’’ paste could only be measured up to a shear rate of 200 s^{-1}. At higher shear rates a pull-off between the paste and the measuring interface appeared. Both sol-based pastes revealed identical viscosity curves and values within the error of the method, varying between 40 Pa s at a shear rate of 1 s^{-1} and 3 Pa s at a shear rate of 1000 s^{-1}. Additionally, a small thixotropic effect is detectable in both curves, which may be traced back to the time-dependent relaxation behavior of the pastes after the higher shear rates of 1000 s^{-1} were applied.

Table 2
Composition of various pastes without binder which fulfill the criteria of homogeneity

Paste type	Sol gel (wt.%)	YSZ oxide powder (wt.%)
Nonanoic sol-based paste	25	75
Nonanoic sol-based paste	35	65
Caproic sol-based paste	20	80
Caproic sol-based paste	30	70
Caproic sol-based paste	25	75

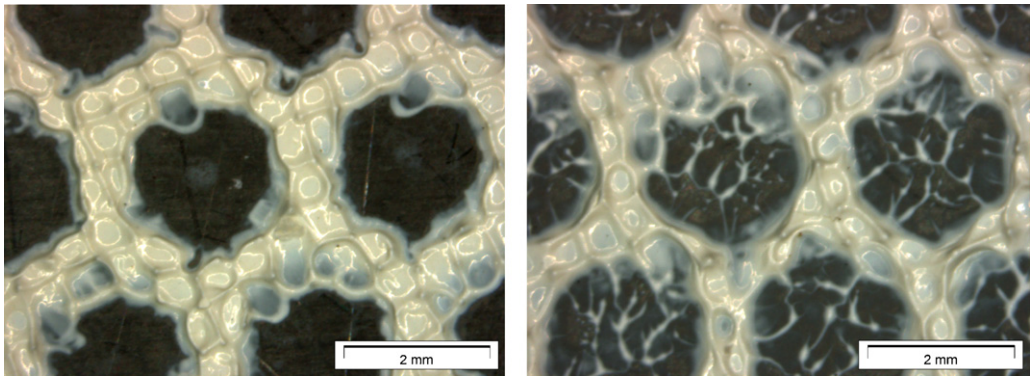

Fig. 4. Screen-printed network of two 8YSZ pastes based on 25 wt.% sol with caproic (left) and nonanoic acid (right) and 75 wt.% mixed-oxide powder.

Table 3
Composition of various pastes with binder which fulfill the criteria of homogeneity

Paste types	Oxide powder (wt.%)	Sol–gel (wt.%)	Binder (wt.%)
"Standard" paste, SP	60	–	40
Caproic-acid-based sol–gel paste	60	20	20
Caproic-acid-based sol–gel paste	60	24	16
Nonanoic-acid-based sol–gel paste	60	20	20
Nonanoic-acid-based sol–gel paste	60	24	16

Table 4
Helium leak rate values for samples with electrolytes based on "standard" 8YSZ paste and composite pastes containing mixed-oxide powder (mo) and a caproic- or nonanoic-based sol [h Pa dm^3/s cm^2]

Paste types	60 wt.% mo powder; 40 wt.% binder	60 wt.% mo powder; 20 wt.% binder; 20 wt.% sol	60 wt.% mo powder; 16 wt.% binder; 24 wt.% sol
"Standard" paste	9×10^{-4}	–	–
Caproic-acid-based sol–gel paste	–	4×10^{-2} 2×10^{-1}	7×10^{-2} 1×10^{-1}
Nonanoic-acid-based sol–gel paste	–	3×10^{-2} 1×10^{-3}	Leakage No value

First printings on SOFC substrates were conducted with a technique where the squeegee displacement is limited to one axis in a back-and-forth movement. With this uniaxial method, 8YSZ films were applied using only pastes with the incorporated binder system, due to the better drying behavior of these materials. In analogy to the rheology measurements, a "standard" paste without a sol was used for comparison. After printing the 8YSZ, the green films were dried and sintered at typical electrolyte sintering conditions of 1400 °C for 5 h. To obtain a first impression of the quality of the layers, the gas-tightness was measured via a helium leak test. While electrolyte layers without an incorporated sol yielded leak rate values of approx. 9×10^{-4} h Pa dm^3/s cm^2, samples coated with a caproic-based sol in the paste showed even higher values in the range of 4×10^{-2} up to 1×10^{-1} h Pa dm^3/s cm^2. Better values are displayed in Table 4, but scattering over a wide range between 1×10^{-3} h Pa dm^3/s cm^2 and complete leakage with no measurable values were observed using pastes based on a nonanoic acid sol.

Due to these results, SEM investigations were carried out on the surfaces of the electrolyte layers to discover the reasons for the measured leak rate values. As can be seen from the typical SEM pictures of the surface in Fig. 5, "standard" paste-printed samples exhibit a crack-free surface with a bimodal grain size distribution and well-developed 120° dihedral angles between the cubic zirconia crystals. Only little intergranular porosity could be detected. In contrast, samples coated with a sol-based electrolyte paste showed a large amount of microcracks on the surface, which could be the origin of the poorer leak rates.

For all the samples the thickness of the sintered electrolyte layer was estimated from cross sections by optical light microscopy. While for nonanoic-based paste and for the "standard" paste without a sol an overall thickness of about 18 and 16 μm was detected, electrolyte layers prepared with a caproic paste yielded a thickness of 12 μm, although the same mesh and the same printing parameters were chosen. No plausible explanation has yet been found for these results.

To avoid the problem of microcracks on the surface of the electrolyte layer in a second set of experiments the substrate was rotated 90° after the forward movement of the squeegee. The experiments were conducted with the pastes and the same

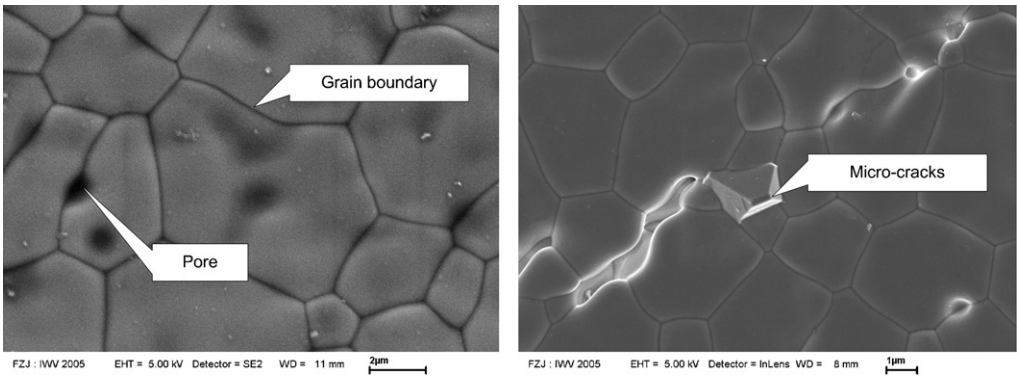

Fig. 5. Typical SEM pictures of surfaces from samples coated with a paste without a sol (left) and a caproic sol-based screen-printing paste (right). Both sintered at 1400 °C for 5 h.

Table 5
Helium leak rate values from transposed printed samples with electrolytes based on standard 8YSZ paste and composite pastes containing mixed-oxide (mo) powder and a caproic- or nonanoic-based sol [h Pa $dm^3/s\ cm^2$]

Paste types	60 wt.% mo powder; 40 wt.% binder	60 wt.% mo powder; 20 wt.% binder; 20 wt.% sol	60 wt.% mo powder; 16 wt.% binder; 24 wt.% sol
Standard paste	3×10^{-6} 4×10^{-4} Leakage, no value	–	–
Caproic-acid-based sol–gel paste	–	4×10^{-6} 1×10^{-5}	1×10^{-4} 9×10^{-5}
Nonanoic-acid-based sol–gel paste	–	1×10^{-5} 9×10^{-6}	3×10^{-5} 2×10^{-5}

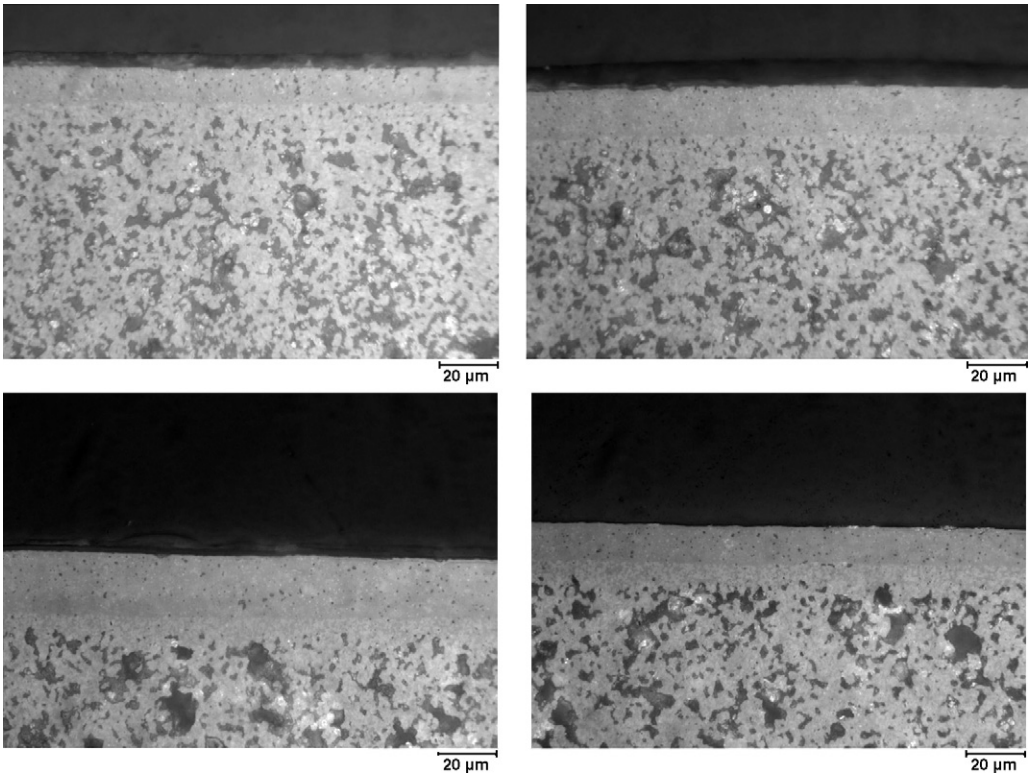

Fig. 6. Optical microscopy pictures of cross-sections of caproic-acid-based (left-hand side top) and a standard uniaxial printed electrolyte (right-hand side top), compared to a nonanoic-acid-based (left-hand side bottom) and a standard transposed printed sample (right-hand side bottom).

sintering parameters that had already been used for the first set of investigations. SEM investigations – not shown here – revealed in all cases structured surfaces without microcracks, which are comparable to those from the "standard" screen-printing paste (left-hand picture in Fig. 5).

All measurements of the layer thickness showed an increase in the layer thickness of up to 20 μm for an electrolyte based on a paste with nonanoic acid and 19 μm for one based on caproic acid in comparison to the thickness of the electrolyte printed in the normal (back and forth) way. In contrast to this increase, samples coated with a paste without an incorporated sol show a decrease of the thickness down to 13 μm. An explanation for this phenomenon could be the faster drying of the sol-based pastes, which results in a higher resistance of the first printed layer. Therefore, the compaction of this layer is not so strong as that of the "standard" paste printed ones. No boundary is visible between the two layers, which could be related to the rotation step (Fig. 6).

In analogy to the uniaxially printed samples, the gas-tightness from the transposed printed samples was estimated by helium leak test measurements. From the results, presented in Table 5, it is obvious that all the samples achieved gas leak rates in the range of or below the internal threshold value of 10^{-5} h Pa $dm^3/s\ cm^2$, which is normally used for standard vacuum slip cast electrolyte layers. It can also be seen that irrespective of the composition of the pastes, all samples exhibit comparable values. A slight decrease of the scattering of the values could be assumed to be caused by the use of a nonanoic-acid-based paste. Investigations of the surface by SEM – not shown here – revealed the same grain size distribution as samples which were uniaxially printed. Microcracks, which were probably the reason for the insufficient gas-tightness of these samples, could not be recognized on the surface of the transposed printed samples. It can be assumed, that the transposed printed second layer covers the remaining failures in the first printed one.

Based on the results of the transposed printed samples, further sintering experiments were conducted on these samples to investigate the influence of lower sintering temperatures on the gas-tightness of the electrolyte layers. Therefore, samples were sintered with the same dwelling time and the same heating rate, but with a 50 °C lower temperature at 1350 °C. Again helium leak rate measurements were conducted, showing that in all cases leak rates higher than the internal threshold value were obtained. While caproic-acid-based sols always have values above the detection limit, samples prepared with a nonanoic-acid-based sol and without a sol showed values in the range of 10^{-3} h Pa $dm^3/s\ cm^2$.

3.3. Single cell tests

Single cell tests were carried out on 50 mm × 50 mm samples with cathodes (a double-layered cathode comprising a first layer composed of 8YSZ and lanthanum–strontium manganate (LSM) as the ceramic electronic conductor and a second layer composed of pure LSM as the current collector) having 40 mm × 40 mm. Cells constructed with electrolyte layers based on sols with caproic and nonanoic acids were prepared (mixtures of sol and oxide powder; transposed printing route). In parallel, samples with a normal electrolyte layer applied by screen printing and sintering to gas-tightness at 1400 °C for 5 h were tested for comparison. The operational conditions were:

Fuel gas: H_2 (3% H_2O) = 1000 ml/min.
Oxidant: air = 1000 ml/min.
Reduction temperature (of the NiO): 900 °C.
Current density measuring temperatures: 650–900 °C.

Figs. 7–9 show the current density–voltage curves obtained and Table 6 lists the current densities at the measured temperatures for better comparison.

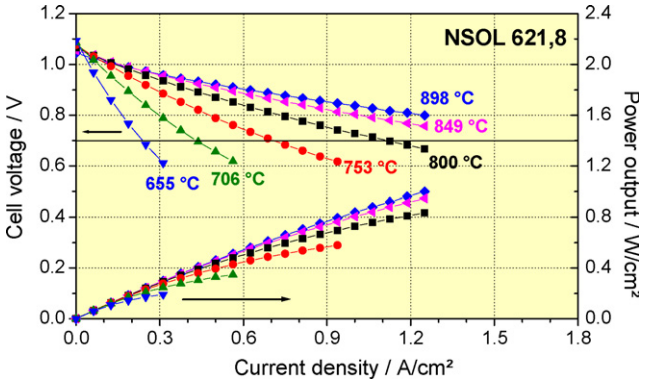

Fig. 7. Current–voltage curves for anode-supported single cell with an electrolyte based on 60% YSZ, 24% nonanoic acid and 16% binder.

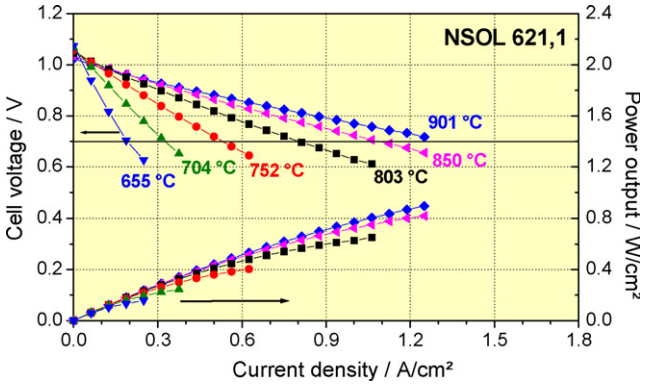

Fig. 8. Current–voltage curves for anode-supported single cell with an electrolyte based on 60% YSZ, 24% caproic acid, and 16% binder.

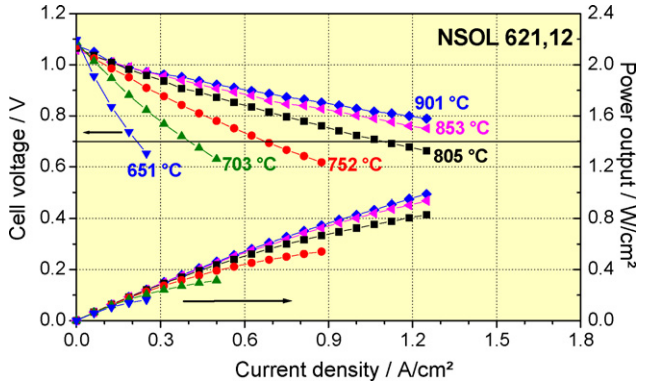

Fig. 9. Current–voltage curves for anode-supported single cell with an electrolyte based on 60% YSZ, 20% nonanoic acid, and 20% binder.

Table 6
Average values of calculated current densities (A/cm^2, 700 mV) as a function of the temperature of the tested anode-supported single cells

Temperature [°C]	Electrolyte with 60% YSZ, 24% nonanoic acid and 16% binder	Electrolyte with 0% YSZ, 24% caproic acid, and 16% binder	Electrolyte with 60% YSZ, 20% nonanoic acid, and 20% binder	Normal electrolyte layer
900	1.72	1.40	1.83	1.83
850	1.43	1.27	1.46	1.53
800	1.05	0.85	1.05	1.09
750	0.67	0.56	0.66	0.67
700	0.39	0.34	0.38	0.39
650	0.23	0.09	0.21	0.21

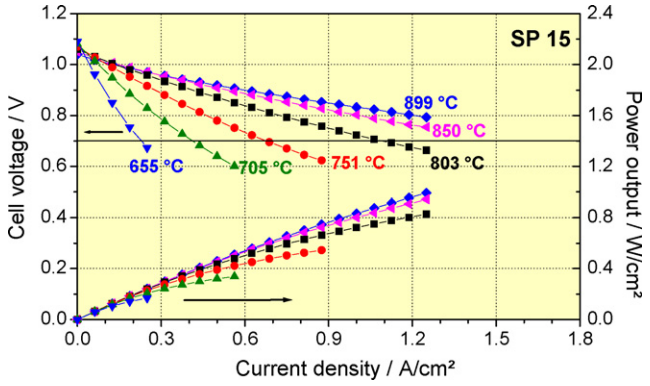

Fig. 10. Current–voltage curves for anode-supported single cell with an electrolyte based on normal screen-printed electrolyte (without sol).

It is obvious that the samples prepared with electrolyte layers based on nonanoic sols have similar current densities to the cells based on the normal wet chemical route (Fig. 10). Cells with an electrolyte layer based on caproic acid show less current density (∼20% less). A possible explanation of the reduced current densities could be that the cells with an electrolyte based on caproic acid have a lower open circuit voltage (OCV) than the other cells tested (1045 mV at 800 °C; others: >1065 mV). A lower OCV is an indicator of some electrolyte leakage. Therefore, a parasitic current passes the cell internally and subsequently reduces the outer current density.

4. Conclusion

Pastes with different ratios of sol–gel and mixed-oxide powder were prepared for screen printing on planar SOFC anode substrates for the deposition of an electrolyte layer. Pastes without a binder system exhibit a very fast and uncontrolled drying behavior. After the incorporation of an organic binder to the sol–gel and the mixed-oxide powder, the prepared pastes exhibited screen-printing ability characteristics. The relation between viscosity, shear rate and recovery of the structure of the paste during screen printing showed the characteristics of conventional pastes used with this printing technique. The electrolyte layers screen printed on anode substrates were sintered at a temperature of 1400 °C, which is a benchmark for attaining gas-tight coatings via a typical vacuum slip casting process. For the different paste application methods, the samples printed using the transposed printing technique exhibited an improved helium leak value, after sintering at 1400 °C.

Those samples printed with the nonanoic-acid-based sol paste (60 wt.% mixed-oxide powder, 20 wt.% binder, 20 wt.% sol) exhibited a helium leak value of 9.3×10^{-6} h Pa dm^3/s cm^2. This value is in the range of the value (3.1×10^{-6} h Pa dm^3/s cm^2) observed for coatings printed with pastes containing only mixed-oxide 8YSZ powder (60 wt.% mixed-oxide powder and 40 wt.% binder).

A reduced margin of error is attributed to those experiments conducted with the nonanoic-acid-based sol pastes, as indicated by the standard deviation of $\pm 1.09 \times 10^{-5}$ h Pa dm^3/s cm^2. Whereas greater divergences were observed in those leak rate values obtained with the caproic-acid-based sol pastes, suggesting difficulties in the process reproducibility.

Furthermore, the pastes screen-printed on anode substrates using the transposed printing application method were sintered at a reduced temperature of 1350 °C and the gas-tightness of those samples did not produce acceptable values. It also follows that only those samples printed with either standard pastes or nonanoic-acid-based sol pastes led to satisfactory results. Even though insufficient gas-tightness was attained from these preliminary results, they provide the basis for further studies.

Single cell tests performed with cells based on electrolytes made with caproic and nonanoic acid sols and printed by the transposed screen-printing method show reasonable to good current densities of approx. 1 A/cm^2. These values are comparable to cells prepared in parallel with a normal screen-printed electrolyte.

References

[1] P. Batfalsky, H.P. Buchkremer, D. Froning, F. Meschke, H. Nabielek, R.W. Steinbrech, F. Tietz:, Operation and analysis of planar SOFC stacks, in: Proc. 3rd IFCC, Nagoya, Japan, (1999), p. 34.
[2] A.A.E. Hassan, N.H. Menzler, G. Blaß, M.E. Ali, H.P. Buchkremer, D. Stöver, Influence of alumina dopant on the properties of yttria-stabilized zirconia for SOFC applications, J. Mater. Sci. 37 (2002) 3447–3475.
[3] H.P. Buchkremer, U. Diekmann, L.G.J. de Haart, H. Kabs, U. Stimming, D. Stöver, Advances in the anode supported planar SOFC technology, in: Proc. 5th Int. Symp. on SOFC, The Electrochemical Society, Pennington, NJ, USA, (1997), pp. 160–170.
[4] N.H. Menzler, R. Hansch, R. Fleck, G. Blaß, H.P. Buchkremer, H. Schichl, D. Stöver, Densification of yttria-stabilized zirconia electrolytes through addition of sintering additives, in: Proc. 8th Int. Symp. on SOFC, The Electrochemical Society, Pennington, NJ, USA, (2003), pp. 238–245.
[5] G.Y. Kim, S.W. Eom, S.I. Moon, Cell properties of SOFC prepared by doctor blade and screen printing method, in: Proc. 5th Int. Symp. on

SOFC, The Electrochemical Society, Pennington, NJ, USA, (1997), pp. 700–709.
[6] G.M. Christie, P. Nammensma, J.P.P. Huijsmans, Status of anode-supported thin electrolyte ceramic SOFC component development at ECN, in: Proc. 4th Europ. SOFC. Forum, Lucerne, Switzerland, (2000), pp. 3–11.
[7] G. Schiller, T. Franco, R. Henne, M. Lang, P. Szabo, O. Finkenwirth, B. Kuhn, F.-J. Wetzel, Development of thin-film SOFC for stationary and mobile applications by using plasma deposition technology, in: Proc. 8th Int. Symp. on SOFC, The Electrochemical Society, Pennington, NJ, USA, (2003), pp. 1051–1058.
[8] D. Stöver, D. Hathiramani, R. Vassen, R.J. Damani, Plasma-sprayed components for SOFC applications, Surf. Coat. Technol. 201 (5) (2006) 2002–2005.
[9] M. Gaudon, N.H. Menzler, E. Djurado, H.P. Buchkremer, YSZ electrolyte of anode-supported SOFCs prepared from sub micron YSZ powders, J. Mater. Sci. 40 (2005) 3735–3743.
[10] R. Hansch, D. Lavergnat, N.H. Menzler, D. Stöver, Nanocrystallized yttria-stabilized zirconia for solid oxide fuel cell applications, Adv. Eng. Mater. 7 (5) (2005) 142–144.
[11] W.A. Meulenberg, N.H. Menzler, H.P. Buchkremer, D. Stöver, Manufacturing routes and state-of-the-art of the planar Jülich anode-supported concept for solid oxide fuel cells, Ceram. Trans. 127 (2002) 99–108.
[12] F. Tietz, H.P. Buchkremer, D. Stöver, Components manufacturing for solid oxide fuel cells, Solid State Ionics 152–153 (2002) 373–381.
[13] D.A. Barrow, T.E. Petroff, SayerF M., Thick ceramic coatings using a sol gel based ceramic-ceramic 0–3 composite, Surf. Coat. Technol. 76–77 (1995) 113–118.
[14] D.A. Barrow, T.E. Petroff, M. Sayer, Method for producing thick ceramic films by a sol gel coating process, US Patent No. 5,585, 136 (1996).
[15] B.L. Cushing, V.L. Kolesnichenko, C.J. O'Connor, Recent advances in the liquid-phase syntheses of inorganic nanoparticles, Chem. Rev. 104 (9) (2004) 3893–3946.